Applied Magnetic Resonance
https://doi.org/10.1007/s00723-021-01347-w

ORIGINAL PAPER

Ferromagnetic Resonance in Permalloy Metasurfaces

N. Noginova[1] · V. Gubanov[2] · M. Shahabuddin[1] · Yu. Gubanova[2] · S. Nesbit[1] · V. V. Demidov[3] · V. A. Atsarkin[3] · E. N. Beginin[2] · A. V. Sadovnikov[2]

Received: 5 March 2021 / Revised: 4 May 2021 / Accepted: 10 May 2021

Abstract
Permalloy films with one-dimensional profile modulation of submicron periodicity are fabricated based on commercially available DVD-R discs and studied using ferromagnetic resonance method and micromagnetic numerical simulations. The main resonance position shows in-plane angular dependence which is strongly reminiscent of that in ferromagnetic films with uniaxial magnetic anisotropy. The main signal and additional low-field lines are attributed to multiple standing spin-wave resonances defined by the grating period. The results may present interest in magnetic metamaterials and magnonics applications.

1 Introduction

Advances in nanofabrication and development of metamaterial concepts bring to life a new class of composite materials whose properties are artificially engineered via responses of nano-features to the electric component of electromagnetic field [1, 2]. Nanoinclusions made from plasmonic metal (silver, gold, aluminum) are commonly used in optical metamaterials due to their strong response to illumination in the range of plasmon resonances [2]. Using magnetic inclusions which respond to the magnetic component of the electromagnetic radiation, one can design magnetic properties and propagation of electromagnetic waves in a material as well [3–8]. In similarity with optical metamaterials [2], such systems can be described in terms of the effective media approximation [9] with the material constants: dielectric permittivity, ε, and magnetic permeability, μ. However, magnetic metamaterials are restricted to the radio frequency range since the dynamic of the magnetic response is relatively slow, with typical frequencies of magnetic resonance in GHz range. On

✉ N. Noginova
noginova@nsu.edu

[1] Norfolk State University, Norfolk, VA 23504, USA

[2] Laboratory "Magnetic Metamaterials", Saratov State University, Saratov 410012, Russia

[3] Kotel'nikov Institute of Radio Engineering and Electronics, RAS, Moscow 125009, Russia

Published online: 18 June 2021

the other hand, the use of magnetic components enables easy tunability of such systems with the external magnetic field. The effective permeability of composites with single-domain small magnetic nanoparticles in polymer matrices can be tuned from negative to positive values [5, 6], presenting interesting opportunities for temporal and spatial control of the wave propagation. Via mutual arrangement of magnetic nanofeatures and their shape, one can design materials with certain anisotropy of magnetic and microwave properties [10–15].

With increased sizes of magnetic features, the effective medium approximation using a single μ might be no longer sufficient as the response to the illumination becomes more complicated due to the excitation and propagation of spin waves. Structures with periodic arrangement of magnetic elements are commonly considered in terms of magnonic crystals [16–24] in analogy with photonic crystals [25–27] exhibiting effective photonic forbidden and allowed bands. In this work we study grating-like permalloy structures with the submicron periodicity. Permalloy is a soft ferromagnetic with high magnetic permeability; it is a common material for various magnetic and magnonic [13, 22–24] studies. In addition, it exhibits plasmonic behavior [28] and an interesting coupling between plasmonic, magnetic and electric properties [29], presenting interest for plasmon-induced magnetization switching and magnetically controlled plasmonics. In our work, we employ the FMR method and micromagnetic numerical simulations to better understand magnetic and magnetic resonance behavior of such systems, applicability of metamaterial description, and a role of spin wave-related effects.

2 Experimental

Our experimental structures are permalloy (Ni–Fe alloy with 80% of Ni and 20% of Fe) thin films with one-dimensional (1D) profile modulation based on the substrates derived from commercially available digital optical storage discs, DVD-R (Digital Video Recordable). The fabrication starts with obtaining polycarbonate grating substrates from disassembling commercial DVD-R by carefully taking out the polymer, plastic, silver, and protective coating layers. Then, permalloy (Py) with a thickness $\delta = 40$ nm is deposited on the prepared and precut DVD substrates using e-beam evaporation. The thickness of the film is independently tested with a profilometer by measuring films simultaneously deposited on glass substrates. Atomic force microscopy (AFM) confirms the profile-modulation parameters, the periodicity $d = 740$ nm and modulation height $h = 60$–80 nm. As main experiments and numerical simulations are performed with Py/DVD structures, for comparison purposes we also prepared permalloy structures with different profile-modulation parameters using substrates derived from discs of the different format, Blu-Ray or CD discs, with $d = 320$ nm and $h = 25$–30 nm in Py/BR structures, and $d = 1600$ nm and $h = 120$–140 nm (Py/CD), see Fig. 1a for the schematics.

Ferromagnetic resonance curves are recorded using the Bruker EPR Spectrometer at 10 GHz microwave frequency (X Band). The sample is placed inside the microwave cavity with the sample orientation corresponding to the external magnetic field, H in plane of the film, Fig. 1b. The direction of the grooves makes an

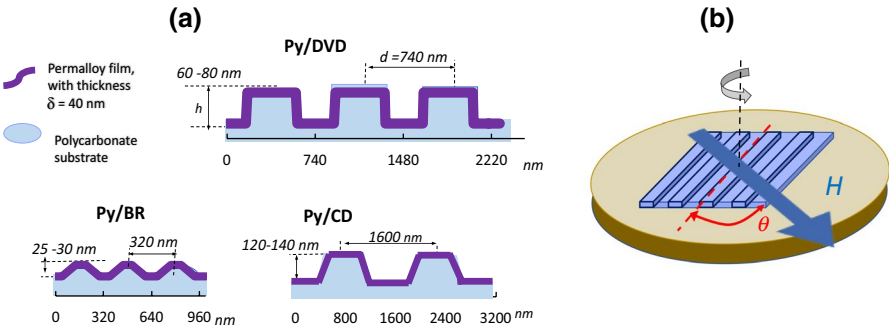

Fig. 1 **a** Profile schematics of Py/DVD, Py/BR, and Py/CD structures (as indicated). **b** Orientation of the sample in FMR experiments

angle θ with H. The signal (the derivative of the microwave absorption vs H) is recorded for various θ.

Typical ferromagnetic resonance spectra observed in Py/DVD are shown in Fig. 2a. (In this plot, the field is shown in Oersted as is in the original recordings.) The signal position depends on the orientation angle, shifting from the lowest to highest field when θ changes from 0 to 90°, corresponding, respectively, to the parallel and perpendicular orientations of the grooves in respect to the external field.

The position of the main FMR peak (determined from fitting with the Lorentzian lines) is plotted as the function of θ, Fig. 2b. The dependence closely follows cos 2θ function. An additional component can be clearly distinguished in some orientations, with the position strongly dependent on the angle as well. The relative strength of this component slightly varies from sample to sample while the angular behavior (Fig. 2c, open circles) follows the same cos 2θ dependence.

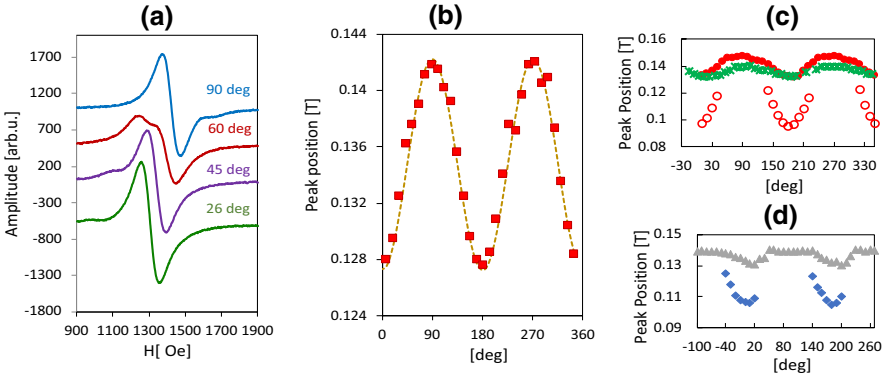

Fig. 2 **a** Typical FMR spectra and **b** position of the main peak as the function of θ in Py/DVD. Dashed trace is fitting with Eq. 1. **c** Peak positions in Py/CD (stars) and Py/DVD (circles), main peak (closed symbols), additional component (open symbols). **d** Positions of two peaks in Py/BR vs angle

We explored the FMR in the other structures as well. A single peak in the Py/CD structures demonstrates the same angular dependence (Fig. 2c, stars) but with a smaller amplitude. The behavior of Py/BR is different. In a broad range of angles ($\theta > 40°$), a single FMR peak is observed with practically no dependence on the orientation. Splitting into two peaks and a strong angular dependence is observed for low angles. Note, that in the current work we concentrate on the Py/DVD system; the other systems will be studied in detail elsewhere.

3 Discussion and Modeling

The angular dependence of the main FMR signal in Py/DVD is strongly reminiscent of that in ferromagnetic films with the growth-induced in-plane uniaxial anisotropy [30, 31]. This can be expected, taking into account that the structural geometry of our gratings is comparable with that of crystalline films [30] but with a submicron-size of the features instead of interatomic distances. Note that films with this type of the magnetic anisotropy exhibit a sharp reorientation of the magnetization upon a small increment of the magnetic field [32, 33], and are of particular interest for optically induced magnetization switching via angular momentum transfer from light to matter [34, 35].

Assuming a relatively small magnetic anisotropy $H_p < H < M$, the FMR condition in our excitation geometry reads [36],

$$\left(\frac{\omega}{\mu_0}\right)^2 \left(H + M + H_p \cos^2\theta\right)\left(H + H_p \cos 2\theta\right), \tag{1}$$

predicting the periodic dependence with the period of 180°, minimum at 0° and maximum at 90° as has been observed in the experiment. Here ω is the FMR frequency, γ is the gyromagnetic ratio, M is the magnetization, and H_p is the anisotropy field [37]. From the fitting with Eq. 1, the effective anisotropy fields are estimated as $\mu_0 H_p = 7.6$ mT in the Py/DVD and 3.7 mT in Py/CD, assuming the saturation magnetization of permalloy, $M = M_S = 6.4 \times 10^5$ A/m. This is in agreement with the literature [12–15] as well, where patterned magnetic structures such as films deposited on the grating-like substrates [13] exhibit a uniaxial anisotropy with the easy axis parallel to the direction of grooves. However, in our Py/DVD systems, additional features are clearly seen, which could not be described with this simple approximation.

In order to better understand magnetic behavior of the Py/DVD structure, we perform numerical simulations, considering a meander-like structure with the following parameters: saturation magnetization of permalloy $M = M_S = 6 \times 10^5$ A/m, periodicity $d = 740$ nm, modulation height $h = 80$ nm, thickness of permalloy, $\delta = 50$ nm at horizontal stages, and various thicknesses $w \leq \delta$ at vertical walls. Since the deposition of metal on the top of the substrate can produce vertical walls with reduced thickness, additional simulations have been performed to explore the role of reduced w. As we found, small variations in the range of possible thicknesses $0 < w \leq \delta$ do not significantly affect the results. The detailed study of FMR behavior in patterned

systems with different parameters including variations in the periodicity, film thickness, and the shape of the profile modulation (sine-wave or rectangular) is the subject of a separate study. In the numerical simulations, we apply an approach discussed in detail in [19] and perform micromagnetic modeling of our structure using the MuMax3 software [38]. The calculation is based on the Landau–Lifshitz–Gilbert equation with damping parameter of 0.007. We consider the same geometry as in the experiment: the external magnetic field lies in plane with the structure and the angle, θ, between the direction of grooves and field varies from 0° to 90. The microwave field with the magnitude of 10^{-4} T is applied along y-axis (perpendicular to the **H** direction).

First, we estimate local distributions of the static magnetization M and effective internal fields H_i (resulting from external and demagnetization fields). In Fig. 3, distributions of H_i (absolute values) are shown at various rotation angles: when the external magnetic field is perpendicular to the direction of grooves (Fig. 3a); makes an angle of 45° (Fig. 3b) or parallel to the grooves (Fig, 3(c)). As one can see, at $\theta = 90°$ and 45°, the magnetic response of the material is strongly modulated in space with maxima of H_i observed in the middle of horizontal stages and minima observed at the corners. The magnitude of this spatial modulation decreases with the decrease in the angle, vanishing at the parallel orientation of the grooves and external field, Fig. 3c. Absorption at the 10 GHz frequency is calculated following the approach [19] as the function of the external magnetic field. In a flat film, a single resonance peak is expected at $\mu_0 H_0 = 0.142$ T, while

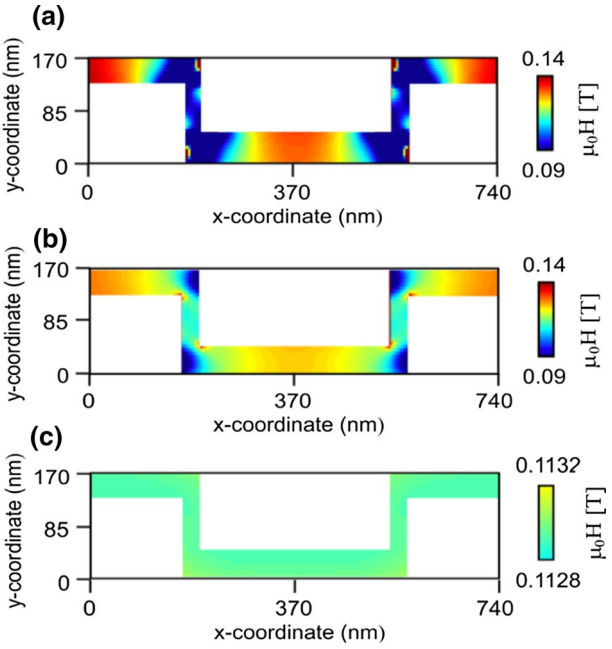

Fig. 3 Distribution of the internal magnetic field at different rotation angles: (a) $\theta = 90°$, (b) $\theta = 45°$, and (c) $\theta = 0^0$. $\mu_0 H_0 = 0.2$ T

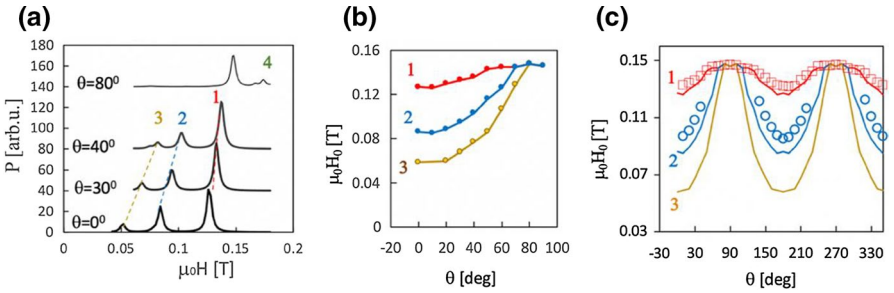

Fig. 4 **a** Simulated microwave (10 GHz) absorption vs field in Py/DVD. **b** Peak positions vs orientation angle, **c** comparison with experiment. Experimental data are shown with symbols, results of numerical simulations are solid traces. Numbers 1, 2, and 3 indicate corresponding peaks

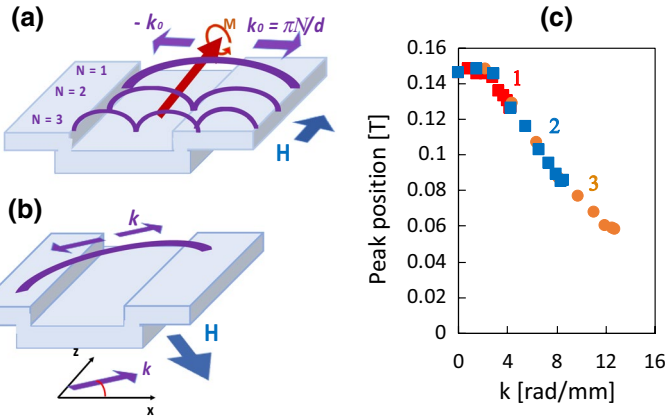

Fig. 5 **a**, **b** Standing modes at **a** perpendicular orientation and **b** an arbitrary angle; **c** Resonance field vs k, simulations. The numbers 1, 2, and 3 indicate corresponding datasets of Fig. 4

in the profile-modulated structures, several peaks can be resolved with the positions dependent on the orientation.

Three major peaks predicted in the Py/DVD structure (with the period $d = 740$ nm and wall thickness $w = 12.5$ nm) are shown in Fig. 4a. With an increase in q, these peaks shift toward H_0, Fig. 4b. The angular dependences for the Peak 1 and Peak 2 positions fairly well correspond to those of the main and additional peaks observed in experiment, Fig. 4c.

Let us assume that the peaks observed below H_0 both in simulations and experiments correspond to the resonance modes formed by the magnetic surface spin waves (MSSW [17–19, 37]) (The Peak 4 in Fig. 4a with the position above H_0 is likely related to the volume modes and is not discussed here). When the field **H** and the magnetization, **M**, are directed along the grooves ($\theta = 0$), MSSW waves are excited in the perpendicular direction, see Fig. 5a which illustrates the amplitude of the precessing transverse magnetization $m(t)$ under the resonance

conditions. Since the spatial modulation (defined by the grating period) has the period of d in this direction, the resonance condition is expected at,

$$k = \pi N/d, \tag{2}$$

where $N = 1, 2, 3...$ is an integer. Standing waves are formed due to the constructive interference of waves reflected from the same type of boundaries (Bragg law). Note that in the frame of magnonic crystal consideration [21], this condition corresponds to the boundaries of the Brillouin zones where the group velocity is zero. An alternative mechanism of the standing wave formation [19] could be considered where an integer number of half-waves fit in horizontal segments (with the length of $\sim d/2$) between groove walls. In this case, an additional factor of 2 should be included in the right side of Eq. (2). As shown below, our data rather indicate that d is the period of modulation. Thus, further we use Eq. (2), though the alternative approach might be applied as well.

When the magnetic field is oriented under an angle θ in respect to the groove direction (Fig. 5b), as an approximation, we assume that the magnetization is directed parallel to the field and spin waves propagate in the orthogonal direction. In this case, the period of the modulation is $d/\cos\theta$, and the k-vector of the resonance mode can be found from the condition,

$$k = N\frac{\pi}{d}\cos\theta. \tag{3}$$

Let us replot the peak position estimated from the numerical calculations (Fig. 4b) as the function of the k-vector estimated from the Eq. 3 with $N = 1$ for the dataset 1, and $N = 2$ and $N = 3$ for the datasets 2 and 3, respectively. All the data fit the single curve (Fig. 5c) confirming our assumptions above. Note, that, alternatively, similar speculations can be applied assuming a twice smaller period $d/2$ of magnetic modulation (which corresponds to the width of each horizontal segment). In this case, the graph (c) will be stretched twice along the x-axis.

In frames of the same numerical approach, the dynamic (transverse) magnetization component m_x is calculated under the resonance conditions of Peaks 1, 2, and 3 at $\theta = 0$. While the absolute values of m_x are symmetric in respect to the middle of the figure (in similarity with Fig. 3), patterns for the instantaneous values are rather complicated, see the panels on the left sides of Fig. 6a–c and their analysis on the right. However, the presence of standing waves is evident, with the k vectors of $\frac{\pi}{d}$, $2\frac{\pi}{d}$, and $3\frac{\pi}{d}$ corresponding to the resonances 1, 2, and 3, respectively. This corresponds to the predictions of Eq. (2).

We put together theory and experiment in Fig. 6d. Points are the experimental results with the abscissas calculated as following: Red circles and triangles: Py/DVD ($d_{\mathrm{DVD}} = 740$ nm). The k vectors are calculated as $k = \frac{\pi}{d_{\mathrm{dvd}}} N\cos\theta$, $N = 1$ for the main peak (circles), and $N = 2$ for the second peak (triangles). Green stars: Py/CD ($d_{\mathrm{CD}} = 1600$ nm). The k vectors are calculated at the same manner assuming $N = 1$, $k = \frac{\pi}{d_{\mathrm{cd}}}\cos\theta$. We make an attempt to add the results obtained in Py/BR ($d_{\mathrm{BR}} = 320$ nm) as well. Points (blue squares) fit the general tendency if we use the second (smaller) peak (which shows strong angular dependence) and estimate $k = \frac{\pi}{d_{\mathrm{BR}}}\cos\theta$. The

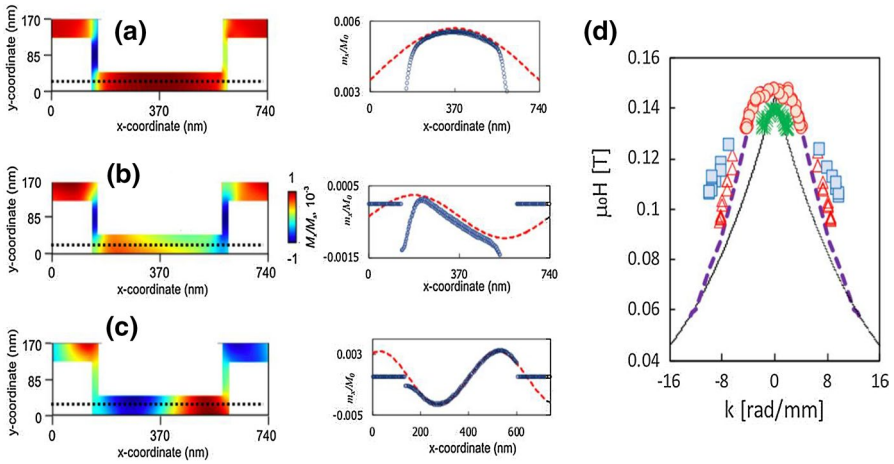

Fig. 6 **a**–**c** Distributions of instantaneous values for dynamic magnetization m_x (left panels) and profiles of m_x along the dotted line (plots on the right) at the resonance conditions of Peaks 1, 2, and 3 at $\theta = 0$, **a** $m_0H = 0.126$ T, **b** $m_0H = 0.0835$ Tm, and **c** $m_0H = 0.052$ T. Red dashed traces are sine waves with the periodicity of **a** $2d$, **b** d, and **c** $2d/3$. **d** Experiment (points) and theory (traces). Py/DVD, main peak (circles), additional peak b: (triangles); Py/CD (stars), Py/BR (squares). Numerical simulations (dashed trace) and predictions for a flat film, Eq. (4) (solid trace)

dashed curve is obtained from the numerical simulations (Fig. 5c). The solid curve is shown for comparison; it is obtained from Eq. (4) which describes the dispersion curve of the MSSW for the flat film [39] with in-plane magnetic field assuming the film thickness $\delta = 50$ nm,

$$\left(\frac{\omega}{\mu_0}\right)^2 = H(H+M) + \frac{M^2}{4}\left(1 - e^{-2k\delta}\right). \tag{4}$$

In principle, assuming a certain relationship between the field and the resonance frequency one can derive the dispersion curve of the spin waves in our structures from the data plotted in Fig. 6. It is already seen that at higher k, the dispersion curve is close to that in a flat film. This is expected since the spin waves with smaller wavelengths are less affected by the profile geometry.

In conclusion, a simple fabrication approach based on commercially available digital storage discs has been suggested and implemented for fabrication of profile-modulated permalloy films. The structures obtained are meander-type parallel grooves with the depth and width on the submicron scale. The ferromagnetic resonance experiments confirm in-plane magnetic anisotropy of structures with the easy axis directed along the grooves and effective anisotropy field of 5–10 mT. Additional low-field resonances are detected as well. We discuss the effects in the frames of the metamaterial approach, show its limitations and a need to take spin waves into account. The presence and behavior of the additional FMR peaks is explained with spin-wave resonances determined by the periodicity of the structures. The findings are confirmed by micromagnetic simulations based on digital solving of the

Landau–Lifshitz Equation with the resonant microwave field taken into account. Both static and dynamic magnetization maps are obtained and used for the analysis of the FMR data. The results can find applications in magnonics, metamaterials and future studies of a possible coupling between surface plasmon polaritons and spin waves.

Acknowledgements N. Noginova, M. Shahabuddin, and S. Nesbit would like to acknowledge financial support from National Science Foundation (NSF) (1830886), Air Force Office of Scientific Research(AFOSR) (FA9550-18-1-0417), and Department of Defence (DoD) (W911NF1810472). The work of authors from Russian Federation is carried out within the framework of the state task and partially was supported by Russian Foundation for Basic Research, project No. 18-57-16001. Micromagnetic simulation of spin-wave resonances was supported by Russian Science Foundation (project No. 20-79-101910).

References

1. J. Haus (ed.), *Fundamentals and Applications of Nanophotonics* (Elsevier, Oxford, 2016), pp. 253–307
2. M.A. Noginov, V.A. Podolskiy (eds.), *Tutorials in Metamaterials* (CRC Press, Boca Raton, 2011), p. 308
3. A.L. Adenot-Engelvin, C. Dudek, P. Toneguzzo, O. Acher, Microwave properties of ferromagnetic composites and metamaterials. J. Eur. Cer. Soc. **27**, 1029–1033 (2007)
4. Y. Poo, R. Wu, G. He, P. Chen, J. Xu, R. Chen, Experimental verification of a tunable left-handed material by bias magnetic fields. Appl. Phys. Lett. **96**, 161902 (2010)
5. C. Morales, J. Dewdney, S. Pal, S. Skidmore, K. Stojak, H. Srikanth, T. Weller, J. Wang, Tunable magneto-dielectric polymer nanocomposites for microwave applications. IEEE Trans. Microw. Theory Tech. **59**, 302–309 (2011)
6. N. Noginova, Q. L. Williams, P. Dallas, E. P. Giannelis, Magnetic nanoparticles for tunable microwave metamaterials, in *Proc. SPIE 8455, Metamaterials: Fundamentals and Applications V*, p. 845531 (2012)
7. M. Mruczkiewicz, M. Krawczyk, R.V. Mikhaylovskiy, V.V. Kruglyak, Towards high-frequency negative permeability using magnonic crystals in meta- material design. Phys. Rev. B **86**(2), 024425 (2012)
8. B. Bates, N. Greene, N. Noginova, Characterization of ferromagnetic/dielectric systems for metamaterials applications, in *Proc. SPIE, 91602R-91602R-4* (2014)
9. T.C. Choy, *Effective Medium Theory* (Clarendon Press, Oxford, 1999).
10. J. Fischbacher, A. Kovacs, H. Oezelt, M. Gusenbauer, D. Suess, T. Schrefl, Effective uniaxial anisotropy in easy-plane materials through nanostructuring. Appl. Phys. Lett. **111**, 192407 (2017)
11. N. Noginova, Yu. Barnakov, A. Radocea, V.A. Atsarkin, Role of dipole-dipole interactions in half-field quantum transitions in magnetic nanoparticles. J. Magn. Magn. Mater. **323**, 2264 (2011)
12. M.O. Liedke, M. Körner, K. Lenz, M. Fritzsche, M. Ranjan, A. Keller, E. Čižmár, S.A. Zvyagin, S. Facsko, K. Potzger, J. Lindner, J. Fassbender, Crossover in the surface anisotropy contributions of ferromagnetic films on rippled Si surfaces. Phys. Rev. B **87**, 024424 (2013)
13. J. Berendt, J.M. Teixeira, A. García-García, M. Raposo, P.A. Ribeiro, J. Dubowik, G.N. Kakazei, D.S. Schmool, Tunable magnetic anisotropy in permalloy thin films grown on holographic relief gratings. Appl. Phys. Lett. **104**, 082408 (2014)
14. R. Moroni, D. Sekiba, F. Buatier de Mongeot, G. Gonella, C. Boragno, L. Mattera, U. Valbus, Uniaxial magnetic anisotropy in nanostructured Co/Cu (001): from surface ripples to nanowires. Phys. Rev. Lett. **91**, 167207 (2003)
15. S.A. Mollick, R. Singh, M. Kumar, S.N. Bhattacharyya, T. Som, Strong uniaxial magnetic anisotropy in Co films on highly ordered grating-like nanopatterned Ge surfaces. Nanotechnology **29**, 125302 (2018)
16. V.V. Kruglyak, S.O. Demokritov, D. Grundler, Magnonics. J. Phys. D Appl. Phys. **43**, 264001 (2010)

17. S.L. Vysotskii, S.A. Nikitov, Yu.A. Filimonov, Magnetostatic spin waves in two-dimensional periodic structures (magnetophoton crystals). J. Exp. Theory Phys. **101**, 547–553 (2005)
18. M.L. Sokolovskyy, M. Krawczyk, The magnetostatic modes in planar one-dimensional magnonic crystals with nanoscale sizes. J. Nanoparticle Res. **13**, 6085–6091 (2011)
19. E.N. Beginin, A.V. Sadovnikov, V.K. Sakharov, A.I. Stognij, Y.V. Khivintsev, S.A. Nikitov, Collective and localized modes in 3D magnonic crystals. J. Magn. Magn. Mat. **492**, 165647 (2019)
20. J.O. Vasseur, L. Dobrzynski, B. Djafari-Rouhani, H. Puszkarski, Magnon band structure of periodic composites. Phys. Rev. B **54**, 1043 (1996)
21. H. Puszkarski, M. Krawczyk, Magnonic crystals—the magnetic counterpart of photonic crystals. Solid State Phenom. **94**, 125 (2003)
22. G. Gubbiotti, L.L. Xiong, F. Montoncello, A.O. Adeyeye, Collective spin waves in arrays of permalloy nanowires with single-side periodically modulated width. Appl. Phys. Lett. **111**, 192403 (2017)
23. P. Malagò, L. Giovannini, R. Zivieri, P. Gruszecki, M. Krawczyk, Spin-wave dynamics in permalloy/cobalt magnonic crystals in the presence of a nonmagnetic spacer. Phys. Rev. B **92**, 064416 (2015)
24. Z.K. Wang, V.L. Zhang, H.S. Lim, S.C. Ng, M.H. Kuok, S. Jain, A.O. Adeyeye, Observation of frequency band gaps in a one-dimensional nanostructured magnonic crystal. Appl. Phys. Lett. **94**, 083112 (2009)
25. J.D. Joannopoulos, P.R. Villeneuve, S. Fan, Photonic crystals: putting a new twist on light. Nature **386**, 143–149 (1997)
26. K. Ohtaka, Energy band of photons and low-energy photon diffraction. Phys. Rev. B. **19**, 5057–5067 (1979)
27. I.A. Sukhoivanov, I.V. Guryev, *Photonic Crystals, Springer Series in Optical Sciences* (Springer Nature, Berlin, 2020), p. 224
28. M. Shahabuddin, N. Noginova, Plasmonic System with In-Plane Magnetic Anisotropy for Plasmon Based Magnetic Switching, OSA Techn. Digests, CLEO: QELS, 2019, paper # JW2A
29. M. Shahabuddin, D. Keene, M. Durach, V. S. Posvyanskii, V. A. Atsarkin N. Noginova, Magnetically dependent plasmon drag in permalloy structures. JOSA B. **38**, 2012–2018 (2021)
30. C. Tang, M. Aldosary, Z. Jiang, H. Chang, B. Madon, K. Chan, M. Wu, J.E. Garay, J. Shi, Exquisite growth control and magnetic properties of yttrium iron garnet thin films. Appl. Phys. Lett. **108**, 102403 (2016)
31. Y.-J. Zhang, L. Wu, J. Ma, Q.-H. Zhang, A. Fujimori, J. Ma, Y.-H. Lin, C.-W. Nan, N.-X. Sun, Interfacial orbital preferential occupation induced controllable uniaxial magnetic anisotropy observed in Ni/NiO(110) heterostructures. Npj Quant. Mater. **2**, 17 (2017)
32. V.A. Atsarkin, V.V. Demidov, A.E. Mefed, VYu. Nagorkin, Magnetic pseudoresonance in manganite thin films. Appl. Magn. Res. **45**, 809–816 (2014)
33. T.M. Vasilevskaya, S.A. Volodin, D.I. Sementsov, Ferromagnetic resonance and bistability field in a uniaxial magnetic film. Tech. Phys. **56**, 1373 (2011)
34. M. Durach, N. Noginova, Spin angular momentum transfer and plasmogalvanic phenomena. Phys. Rev. B **96**, 195411 (2017)
35. K.Y. Bliokh, A.Y. Bekshaev, F. Nori, Optical momentum and angular momentum in complex media: from the Abraham-Minkowski debate to unusual properties of surface plasmon-polaritons. New J. Phys. **19**, 123014 (2017)
36. V.V. Demidov, I.V. Borisenko, A.A. Klimov, G.A. Ovsyannikov, A.M. Petrzhik, S.A. Nikitov, Magnetic anisotropy in strained manganite films and bicrystal junctions. JETP **112**, 825 (2011)
37. A.G. Gurevich, G.A. Melkov, *Magnetization Oscillation and Waves* (CRC, New York, 1996).
38. A. Vansteenkiste, J. Leliaert, M. Dvornik, M. Helsen, F. Garcia-Sanchez, B. Van Waeyenberge, The design and verification of MuMax3. AIP Adv. **4**, 107133 (2014)
39. D.D. Stancil, *Theory of Magnetostatic Waves* (Springer, Berlin, 2012).

Terms and Conditions

Springer Nature journal content, brought to you courtesy of Springer Nature Customer Service Center GmbH ("Springer Nature").

Springer Nature supports a reasonable amount of sharing of research papers by authors, subscribers and authorised users ("Users"), for small-scale personal, non-commercial use provided that all copyright, trade and service marks and other proprietary notices are maintained. By accessing, sharing, receiving or otherwise using the Springer Nature journal content you agree to these terms of use ("Terms"). For these purposes, Springer Nature considers academic use (by researchers and students) to be non-commercial.

These Terms are supplementary and will apply in addition to any applicable website terms and conditions, a relevant site licence or a personal subscription. These Terms will prevail over any conflict or ambiguity with regards to the relevant terms, a site licence or a personal subscription (to the extent of the conflict or ambiguity only). For Creative Commons-licensed articles, the terms of the Creative Commons license used will apply.

We collect and use personal data to provide access to the Springer Nature journal content. We may also use these personal data internally within ResearchGate and Springer Nature and as agreed share it, in an anonymised way, for purposes of tracking, analysis and reporting. We will not otherwise disclose your personal data outside the ResearchGate or the Springer Nature group of companies unless we have your permission as detailed in the Privacy Policy.

While Users may use the Springer Nature journal content for small scale, personal non-commercial use, it is important to note that Users may not:

1. use such content for the purpose of providing other users with access on a regular or large scale basis or as a means to circumvent access control;
2. use such content where to do so would be considered a criminal or statutory offence in any jurisdiction, or gives rise to civil liability, or is otherwise unlawful;
3. falsely or misleadingly imply or suggest endorsement, approval , sponsorship, or association unless explicitly agreed to by Springer Nature in writing;
4. use bots or other automated methods to access the content or redirect messages
5. override any security feature or exclusionary protocol; or
6. share the content in order to create substitute for Springer Nature products or services or a systematic database of Springer Nature journal content.

In line with the restriction against commercial use, Springer Nature does not permit the creation of a product or service that creates revenue, royalties, rent or income from our content or its inclusion as part of a paid for service or for other commercial gain. Springer Nature journal content cannot be used for inter-library loans and librarians may not upload Springer Nature journal content on a large scale into their, or any other, institutional repository.

These terms of use are reviewed regularly and may be amended at any time. Springer Nature is not obligated to publish any information or content on this website and may remove it or features or functionality at our sole discretion, at any time with or without notice. Springer Nature may revoke this licence to you at any time and remove access to any copies of the Springer Nature journal content which have been saved.

To the fullest extent permitted by law, Springer Nature makes no warranties, representations or guarantees to Users, either express or implied with respect to the Springer nature journal content and all parties disclaim and waive any implied warranties or warranties imposed by law, including merchantability or fitness for any particular purpose.

Please note that these rights do not automatically extend to content, data or other material published by Springer Nature that may be licensed from third parties.

If you would like to use or distribute our Springer Nature journal content to a wider audience or on a regular basis or in any other manner not expressly permitted by these Terms, please contact Springer Nature at

onlineservice@springernature.com